Electronic Supplementary Material (ESI) for Journal of Materials Chemistry A.

Incorporation of Free Halide Ions Stabilizes Metal–Organic Frameworks (MOFs) Against Pore Collapse and Renders Large-pore Zr-MOFs Functional for Water Harvesting

Zhiyong Lu,*[a][b]† Jiaxin Duan,[b]† Liting Du,[c] Qin Liu,[b] Neil Schweitzer[d] and Joseph T. Hupp*[b]

[a]College of Mechanics and Materials, Hohai University, Nanjing 210098, China
[b]Department of Chemistry, Northwestern University, 2145 Sheridan Road, Evanston, Illinois 60208, USA
[c]Advanced Analysis and Testing Center, Nanjing Forestry University, Nanjing 210037, China
[d]Department of Chemical Engineering, Northwestern University, 2145 Sheridan Road, Evanston, Illinois 60208, USA

Table of contents

1. Materials and General Methods

Materials. All reagents were obtained from commercial vendors and, unless otherwise noted, were used without further purification.

Physical Methods and Instrumentation.

N_2 isotherms were collected on a Micromeritics Tristar II 3020 instrument at 77 K. Pore-size distributions were calculated from these isotherms using a carbon split-pore model with a N_2 kernel. Water adsorption isotherms were performed using a Micromeritics 3Flex instrument in the Reactor Engineering and Catalyst Testing (REACT) core facility at Northwestern University. The samples were maintained at 25 °C using a Micromeritics ISO controller, the water source was maintained at 35 °C. In full isotherms, adsorption and desorption data points were collected from 0.05 – 0.9 relative pressure every 0.02 units using an equilibration interval of 10 s. Cycling measurements were made by cycling directly from 0.1 to 0.8 relative pressure using an equilibration interval of 10 s.

Diffuse reflectance infrared Fourier transform spectra (DRIFTS) were recorded on a Nicolet 7600 FT-IR spectrometer equipped with an MCT/A detector. Samples diluted in KBr were measured with a KBr background and kept at each temperature under Ar purge (samples prepared in atmosphere). The spectra were collected at 1 cm^{-1} resolution and 32 scans were averaged over the spectral window of 675–4000 cm^{-1}.

Powder X-ray diffraction (PXRD) patterns were measured at room temperature on a STOE-STADIMP powder diffractometer equipped with an asymmetric curved Germanium monochromator (CuKα1 radiation, λ = 1.54056 Å) and one-dimensional silicon strip detector (MYTHEN2 1K from DECTRIS). The line focused Cu X-ray tube was operated at 40 kV and 40 mA. The activated powder was sandwiched between two Kapton foils and measured in transmission geometry in a rotating holder. Intensity data from 2 to 30 degrees two theta were collected over a period of 6 min. The instrument was calibrated against a NIST Silicon standard (640d) prior to the measurement.

Scanning electron micrographs (SEM) images were taken using a Hitachi SU8030/S-4800 and JEOL JSM-7900FLV at the EPIC facility (NUANCE Center-Northwestern University). EDS Map scans were obtained on the same instrument.

Synthesis of MOF-808-Formate. The synthesis of bulk microcrystalline powder MOF-808-Formate was performed according to a reported procedure.[1] Briefly, 0.48 g $ZrOCl_2.8H_2O$ and 0.33 g 1,3,5-1,3,5-Tricarboxybenzene were dissolved in DMF (60 mL), and then 60 mL formic acid was added. The solution was kept in an oven at 100 °C for 48 h, yielding white polycrystalline. The white sample was washed with DMF for at least 5 times to remove trapped modulators and linkers from the pore (50 mL each; soaking ~1 h between washes), and then solvent-exchanged with acetone three times (50 mL each; soaking ~1 h between washes) and soaked in acetone for an additional 16 h. MOF-808-Formate sample was collected by centrifugation, dried in a vac. oven (80 °C for 1 h), and activated at 120 °C for 18 h under dynamic vacuum to yield white powder.

MOF-808-Cl. About 40 mg of as-synthesized MOF-808-Formate sample was solvent-exchanged with Dioxane for at least 5 times over the course of 24 h to remove DMF from the pore. The white solid was then dispersed in a soln. of 12 mL of Dioxane and 0.24 mL of 8M aqueous HCl. The mixture was kept at room temperature for 18 h. Then, the solid was isolated by centrifugation and washed with Dioxane over the course of 8 h (4 × 12 mL). The powder sample was further solvent-exchanged with acetone three times (15 mL each; soaking ~1 h between washes) and soaked in acetone for an additional 16 h. The MOF-808-Cl sample was collected by centrifugation, dried in a vac. oven (80 °C for 1 h), and activated at 120 °C for 18 h under dynamic vacuum to yield white powder.

MOF-808-Br. About 40 mg of as-synthesized MOF-808-Formate sample was solvent-exchanged with Dioxane for at least 5 times over the course of 24 h to remove DMF from the pore. The white precipitate was then dispersed in 12 mL of Dioxane and 0.24 mL of 8M aqueous HBr. The mixture was kept at room temperature for 18 h. The white polycrystalline material was collected into centrifuge tubes and washed with Dioxane over the course of 8 h (4 × 12 mL). The powder sample was further solvent-exchanged with acetone three times (15 mL each, with ~1 h of soaking between washes) and soaked in acetone for an additional 16 h. The MOF-808-Br sample was collected by centrifugation and dried in a vacuum oven at 80 °C for 1 h, and then thermally activated at 120 °C for 18 h under dynamic vacuum to yield grey powder.

MOF-808-I. About 40 mg of as-synthesized MOF-808-Formate sample was solvent-exchanged with Dioxane for at least 5 times over the course of 24 h to remove DMF from the pore. The white precipitate was then dispersed in 12 mL of Dioxane and 0.24 mL of 8M aqueous HI. The mixture was kept at room temperature for 18 h. The white polycrystalline material was collected into centrifuge tubes and washed with Dioxane over the course of 8 h (4 × 12 mL). Further washings were conducted when ^{1}H NMR spectra of digesting sample showed the incomplete removal of formate. The powder sample was further solvent-exchanged with acetone three times (15 mL each, with ~1 h of soaking between washes) and soaked in acetone for an additional 16 h. The MOF-808-I sample was collected by centrifugation and dried in a vacuum oven at 80 °C for 1 h, and then thermally activated at 120 °C for 18 h under dynamic vacuum to yield brown powder.

2. Characterization of MOF-808-Formate and its water adsorption

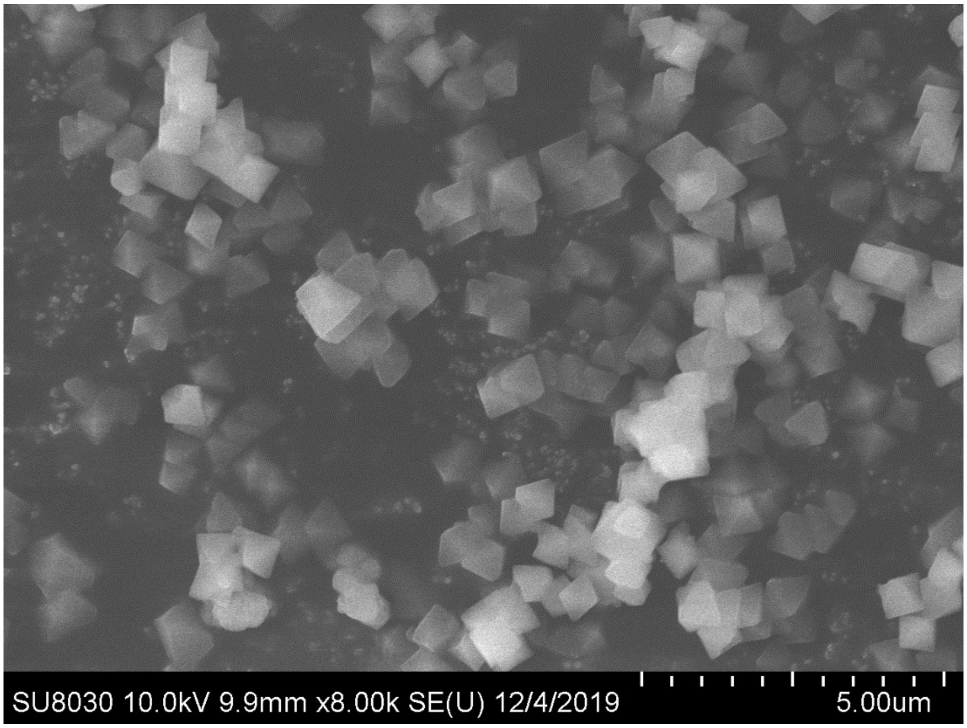

Figure S1. Scanning Electron Microscopy (SEM) image of **MOF-808-Formate**.

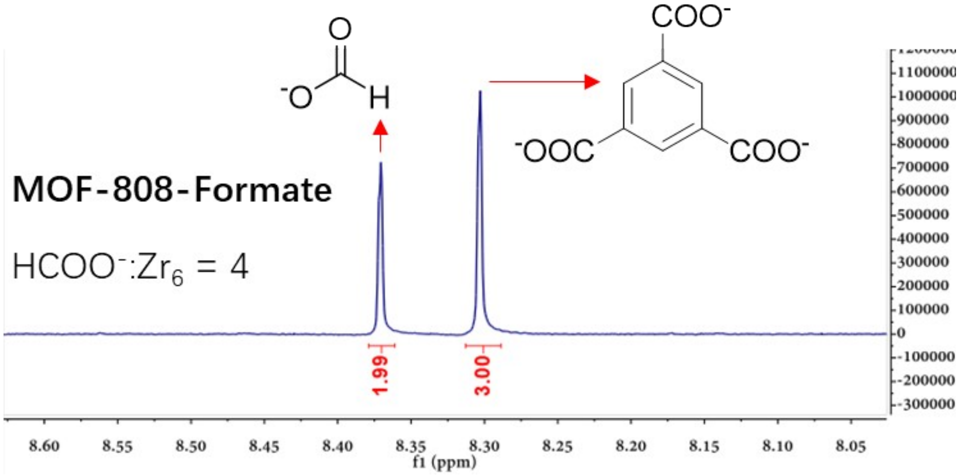

Figure S2. ^1H NMR spectrum of **MOF-808-Formate** digested in 0.1 M $NaOD/D_2O$ and diluted in D_2O. There are about 4 formate (at 8.37 ppm) ions per Zr_6 node.

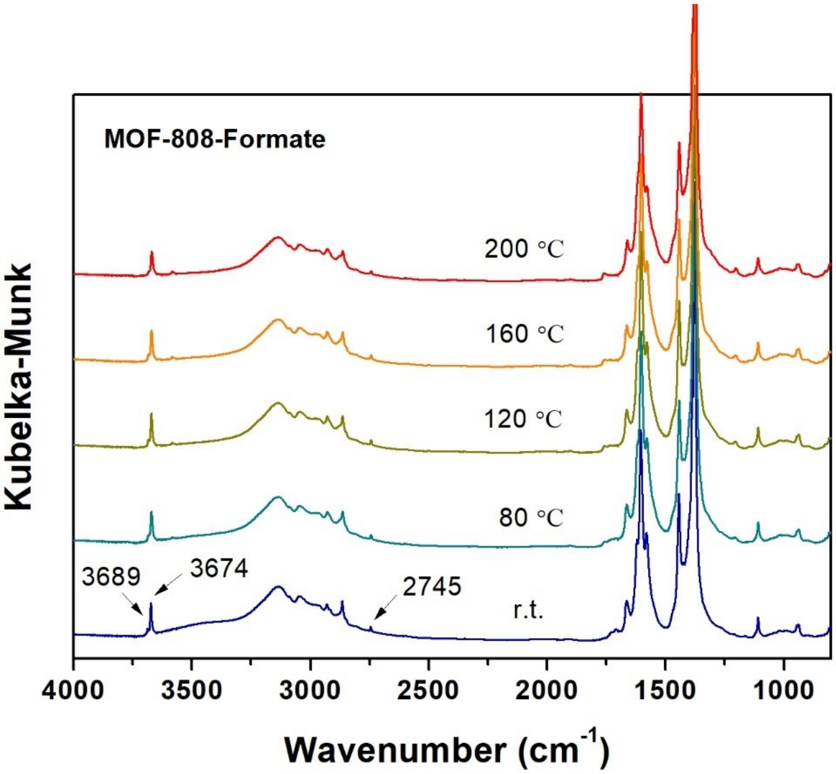

Figure S3. DRIFTS of **MOF-808-Formate** under different temperatures in Ar atomosphere.

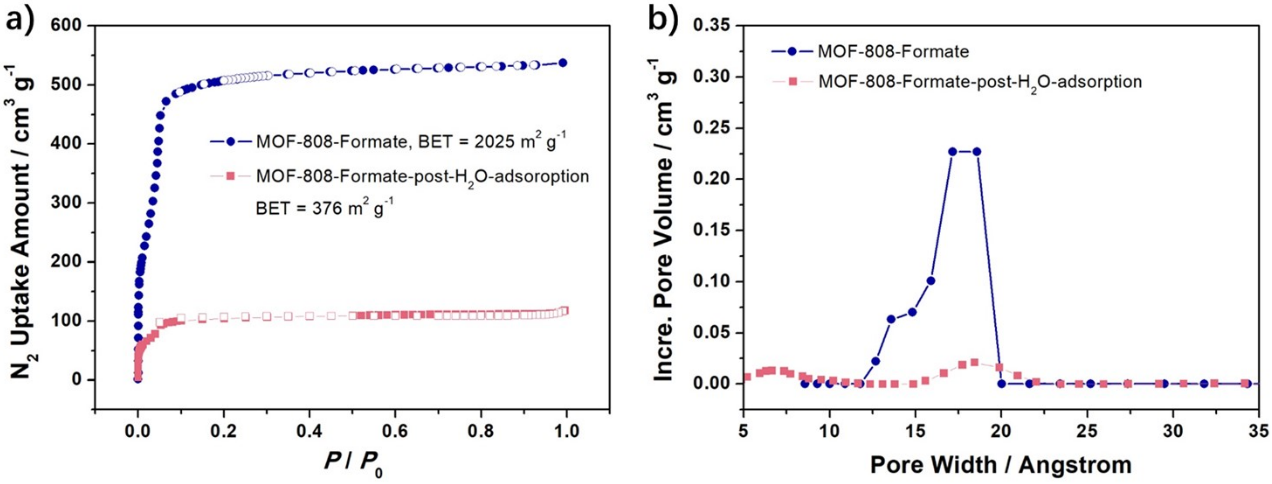

Figure S4. a) Nitrogen adsorption isotherms and b) Pore size distributions of **MOF-808-Formate** and **MOF-808-Format** after 3 cycles of water adsorption.

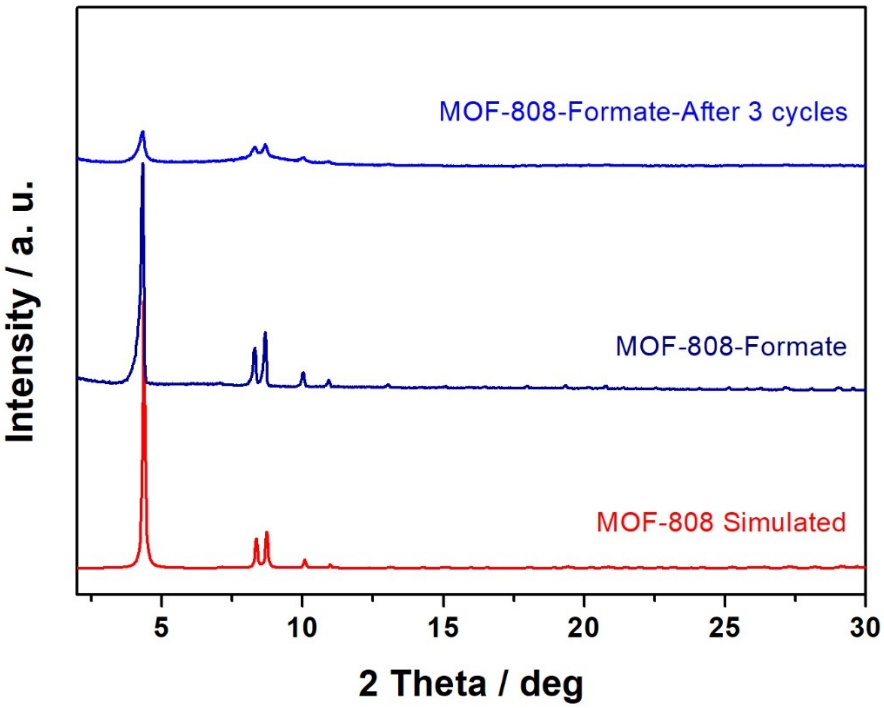

Figure S5. PXRD patterns of **MOF-808-Formate** (navy) and simulated (red).

3. MOF-808-Cl and its water adsorption

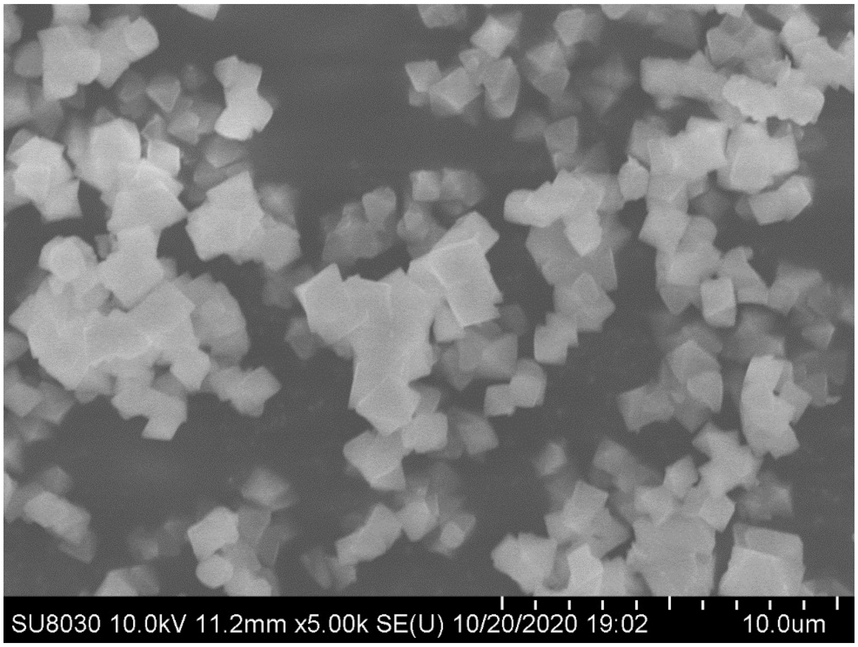

Figure S6. Scanning Electron Microscopy (SEM) image of **MOF-808-Cl**.

.

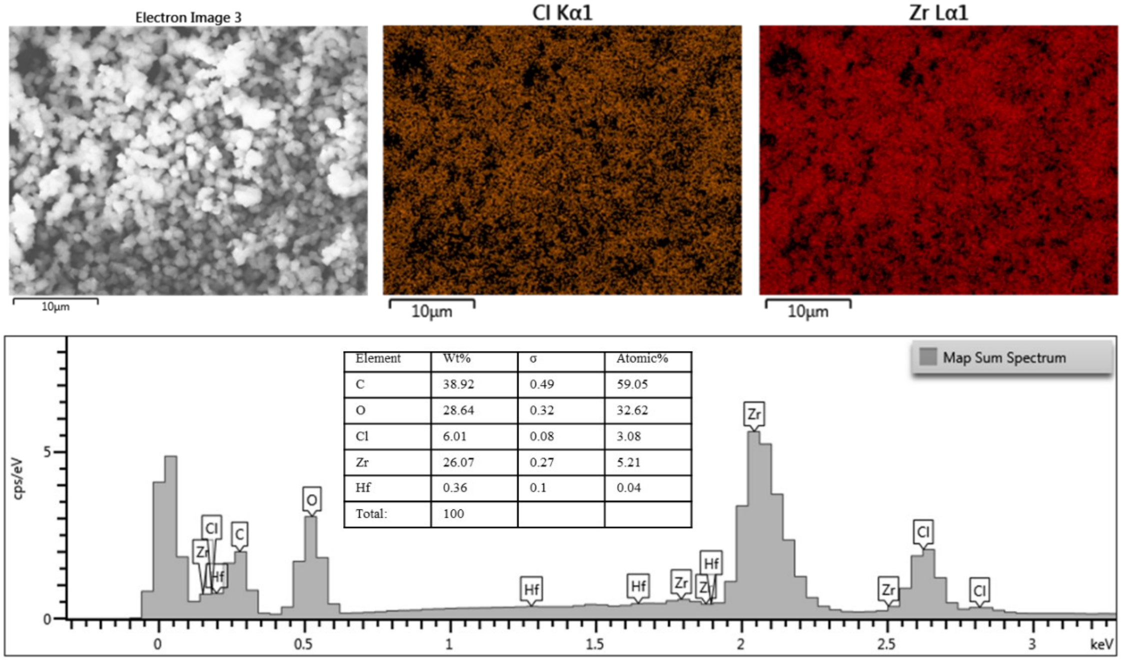

Element	Wt%	σ	Atomic%
C	38.92	0.49	59.05
O	28.64	0.32	32.62
Cl	6.01	0.08	3.08
Zr	26.07	0.27	5.21
Hf	0.36	0.1	0.04
Total:	100		

Figure S7. SEM-EDS mapping of **MOF-808-Cl** showing the evenly distribution of Cl.

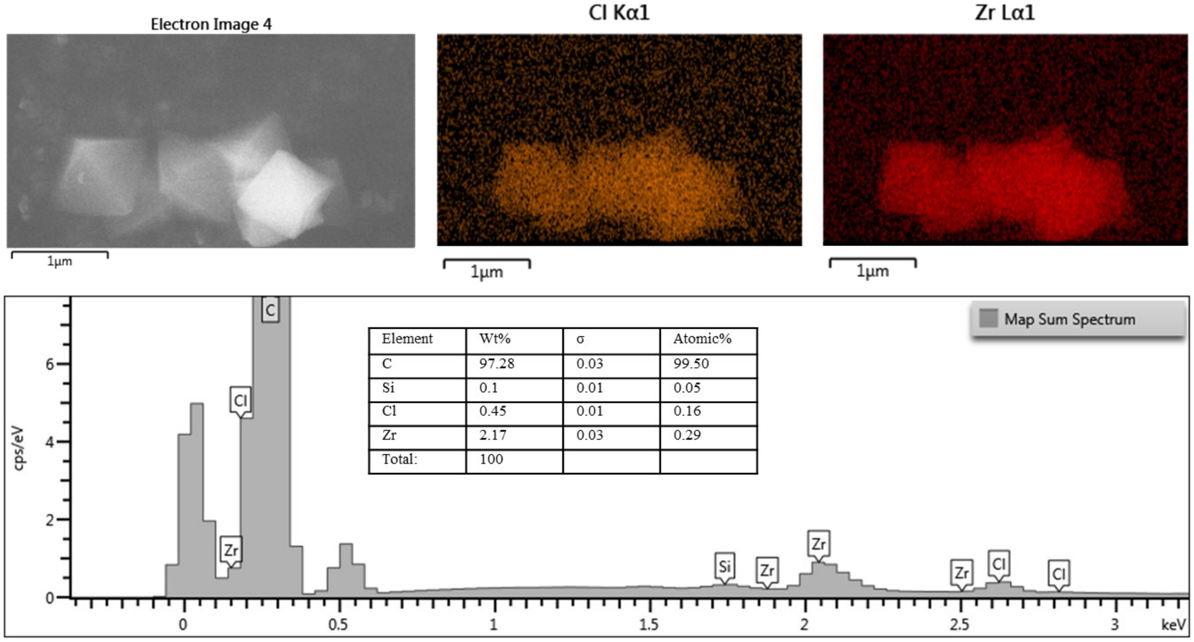

Element	Wt%	σ	Atomic%
C	97.28	0.03	99.50
Si	0.1	0.01	0.05
Cl	0.45	0.01	0.16
Zr	2.17	0.03	0.29
Total:	100		

Figure S8. SEM-EDS mapping of **MOF-808-Cl** showing the evenly distribution of Cl in the crystals.

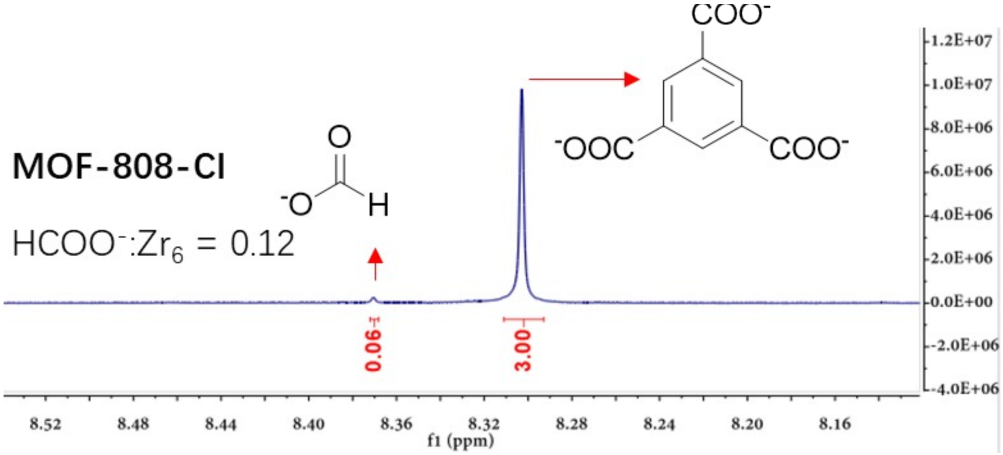

Figure S9. ^{1}H NMR spectrum of **MOF-808-Cl** digested in 0.1 M NaOD/D_2O and diluted in D_2O. There are about 0.12 formate (at 8.37 ppm) left on each Zr_6 node.

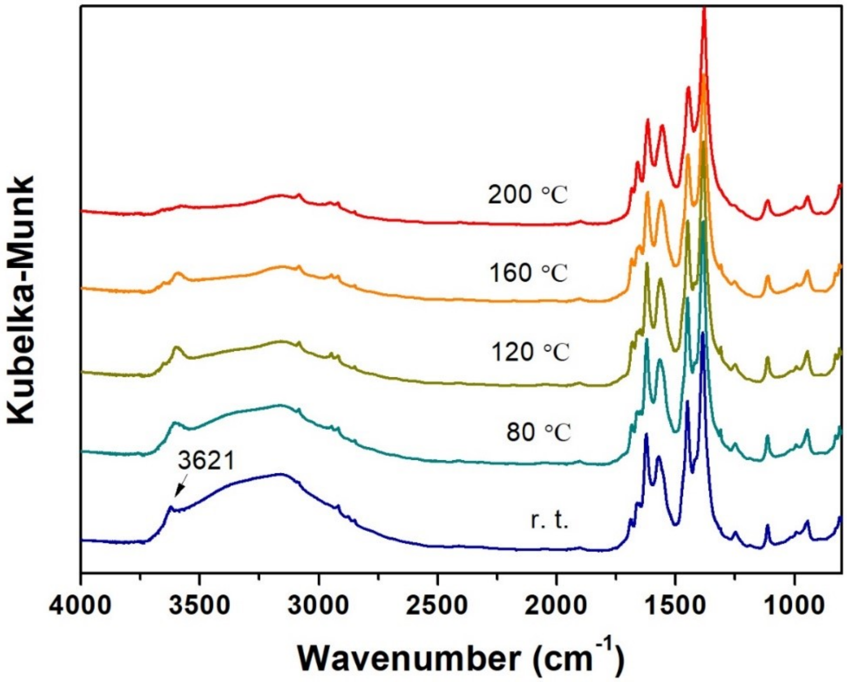

Figure S10. DRIFTS of **MOF-808-Cl** under different temperatures in Ar atomosphere.

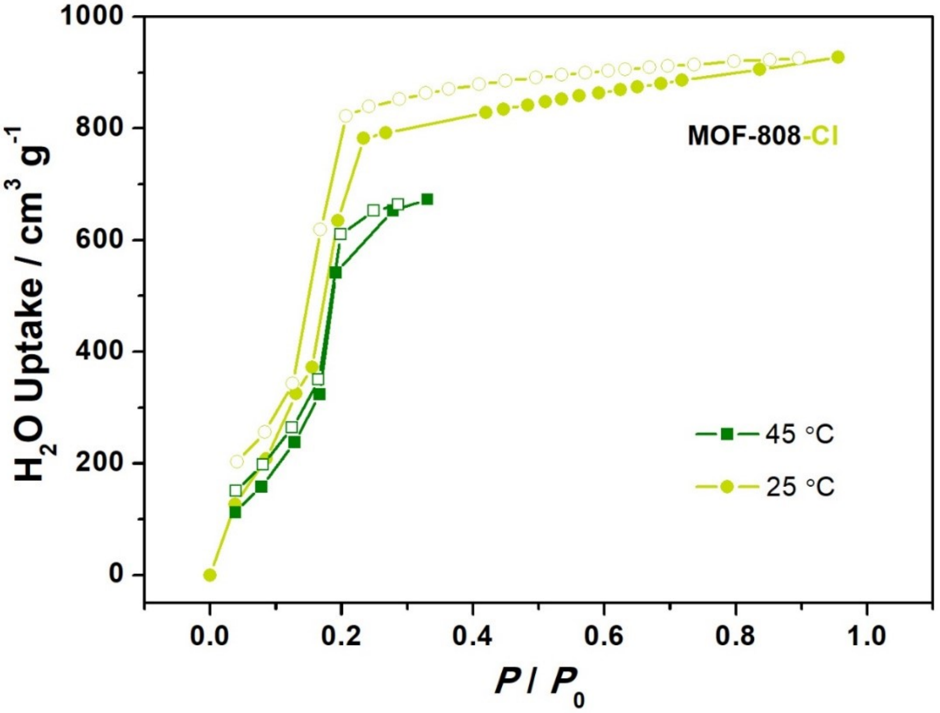

Figure S11. Water adsorption isotherms of **MOF-808-Cl** at 25 °C and 45 °C.

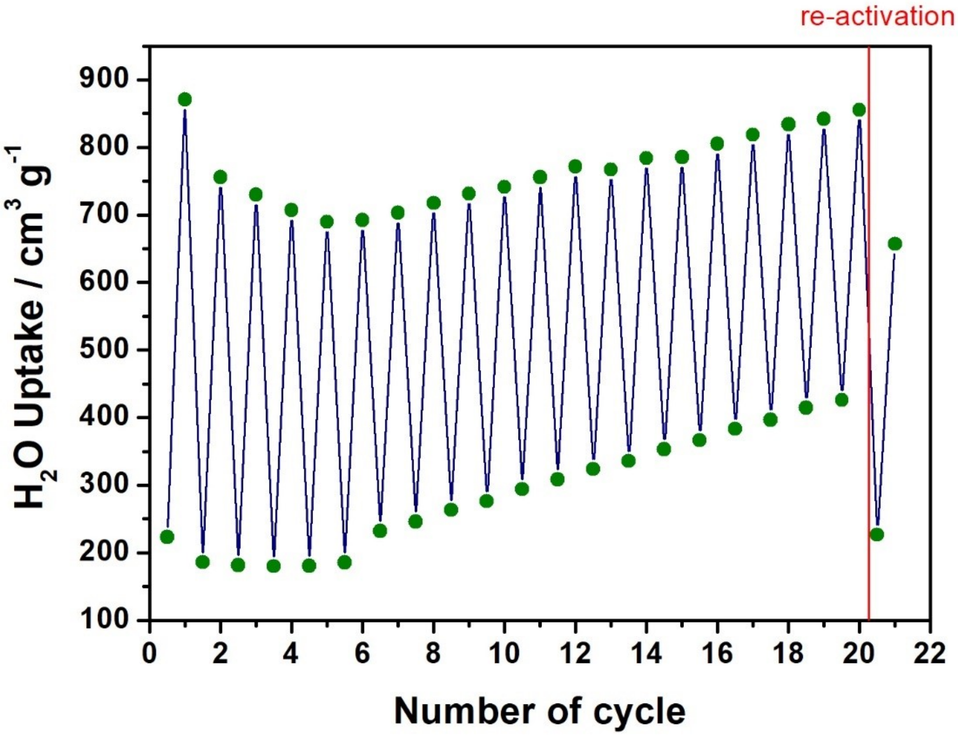

Figure S12. The two-points cycle stability test of **MOF-808-Cl**; $P/P_0 = 0.1$ and 0.8, respectively. The 21st cycle was done after re-activation of the sample at 80 °C under dynamic vacuum for 12h.

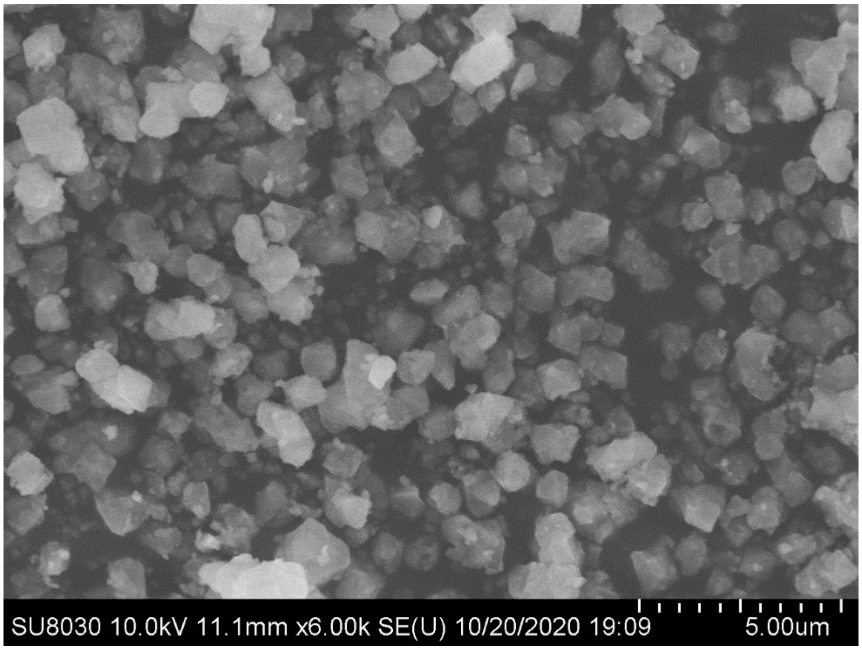

Figure S13. Scanning Electron Microscopy (SEM) image of **MOF-808-Cl** after 20 cycles of water adsorption.

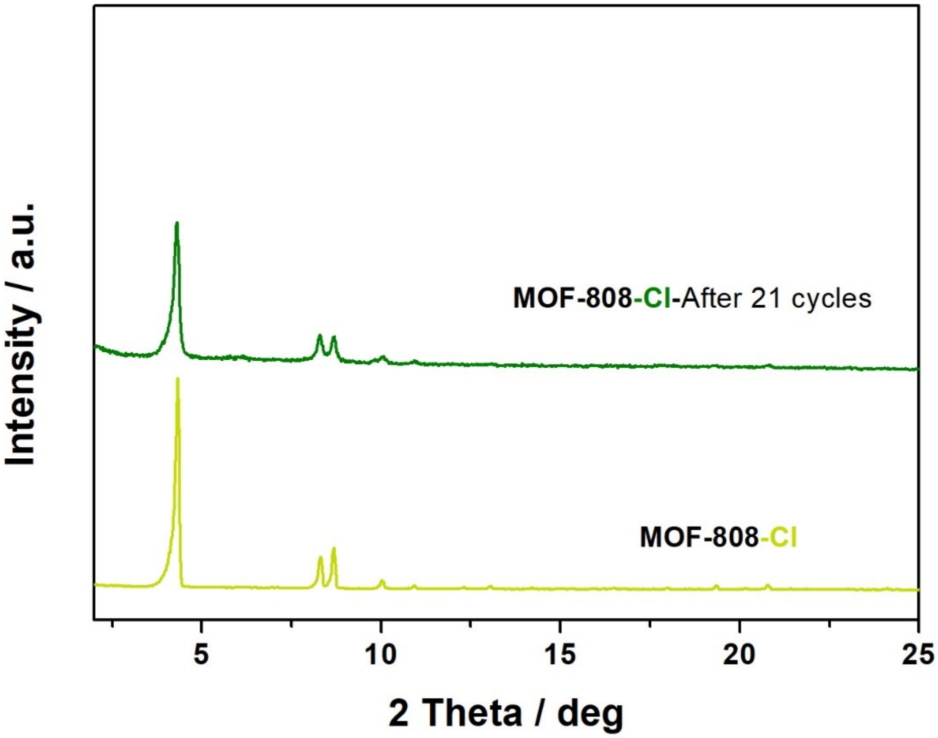

Figure S14. PXRD patterns of MOF-808-Cl before water adsorption and after 21cycles of water adsorption.

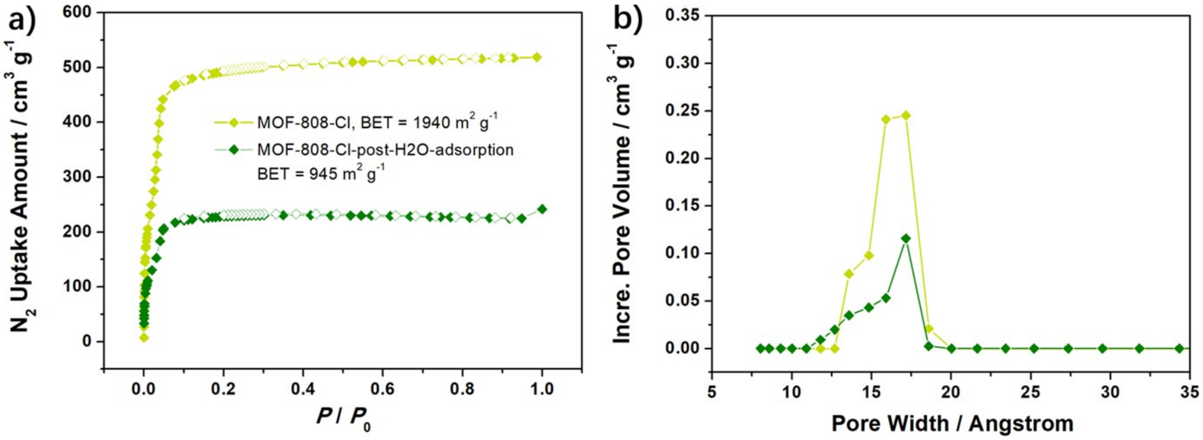

Figure S15. a) Nitrogen adsorption isotherms and b) Pore size distributions of **MOF-808-Cl** and **MOF-808-Cl** after 21 cycles of water adsorption.

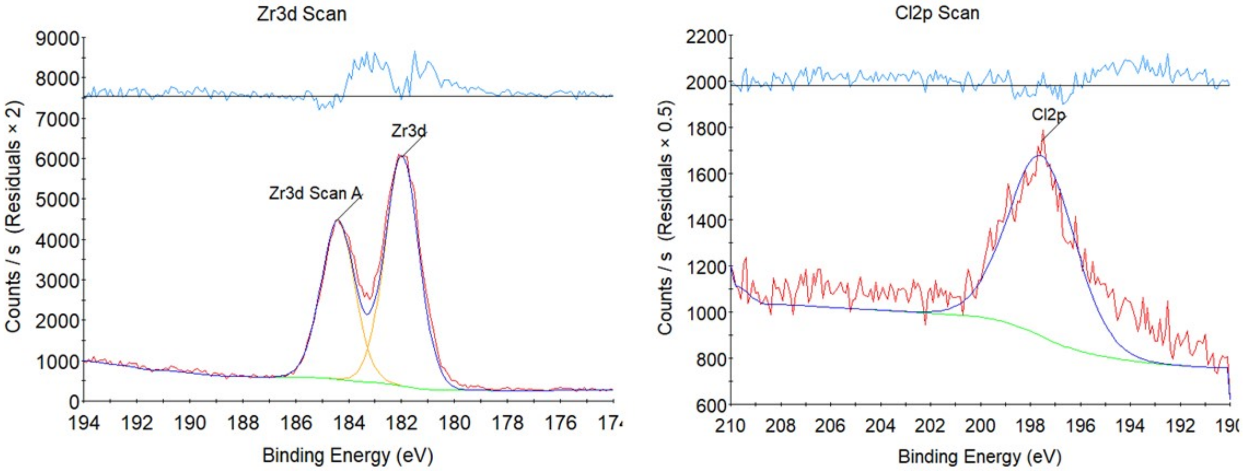

Figure S16. XPS of **MOF-808-Cl**. The binding energy of Cl is 197.6 eV.

4. MOF-808-Br and its water adsorption

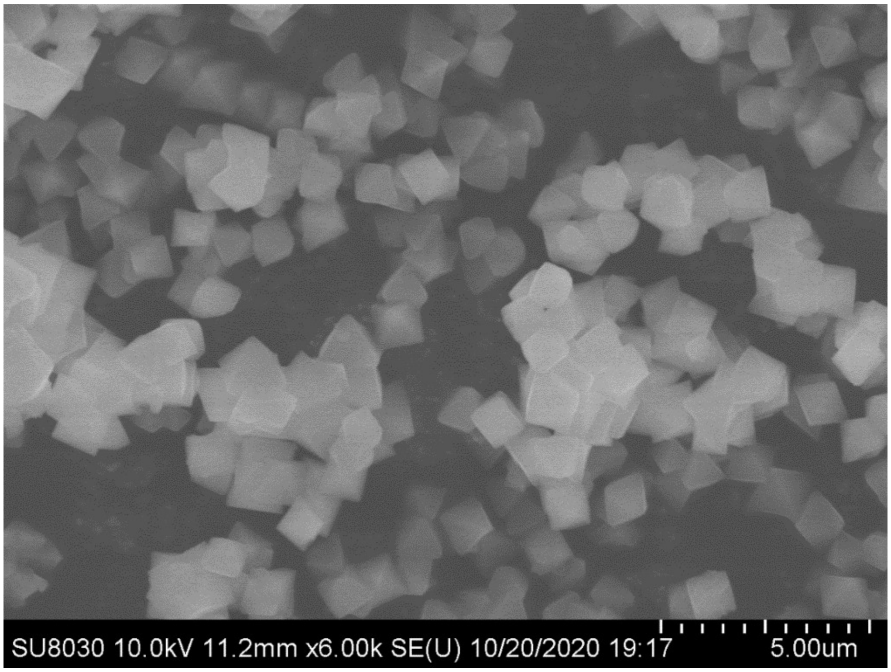

Figure S17. Scanning Electron Microscopy (SEM) image of **MOF-808-Br**.

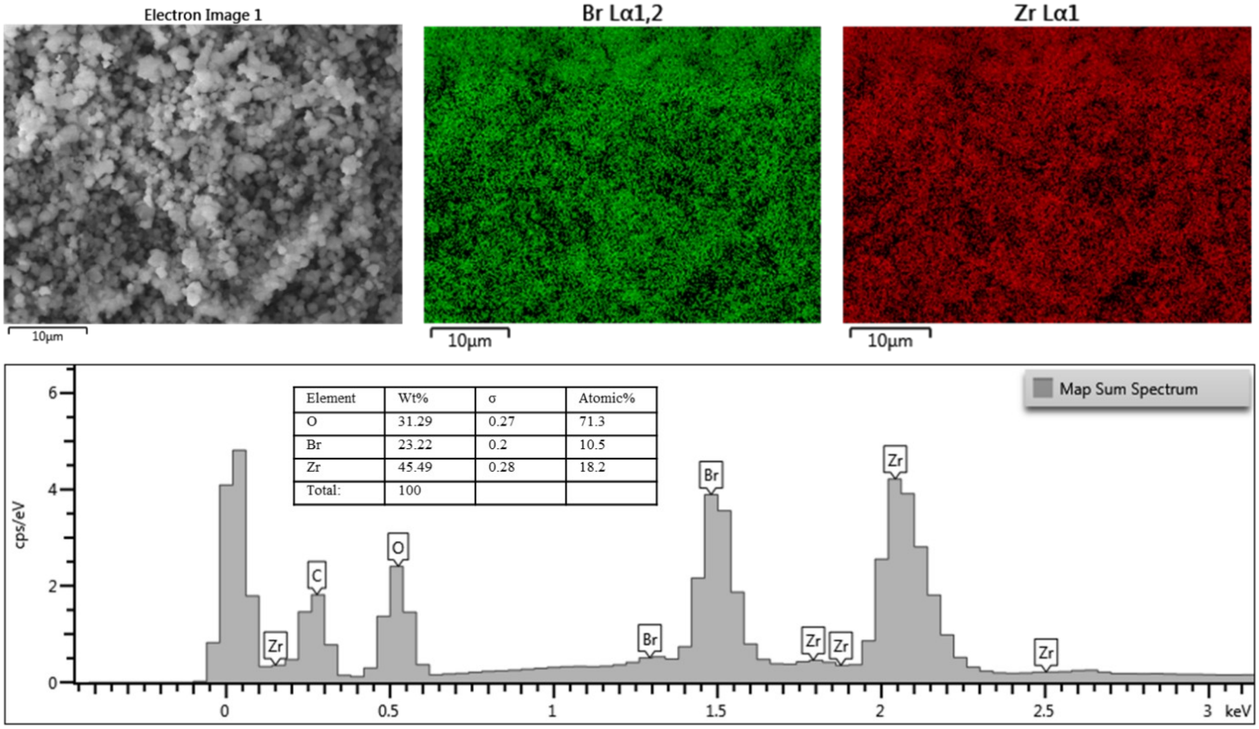

Element	Wt%	σ	Atomic%
O	31.29	0.27	71.3
Br	23.22	0.2	10.5
Zr	45.49	0.28	18.2
Total:	100		

Figure S18. SEM-EDS mapping of **MOF-808-Br** showing the evenly distribution of Br.

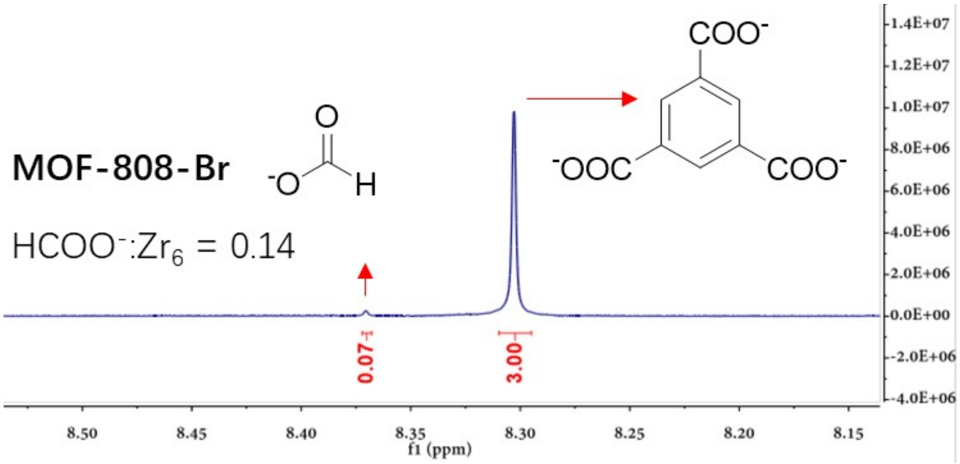

Figure S19. ^{1}H NMR spectrum of **MOF-808-Br** digested in 0.1 M NaOD/D_2O and diluted in D_2O. There are about 0.14 formate (at 8.37 ppm) left on each Zr_6 node.

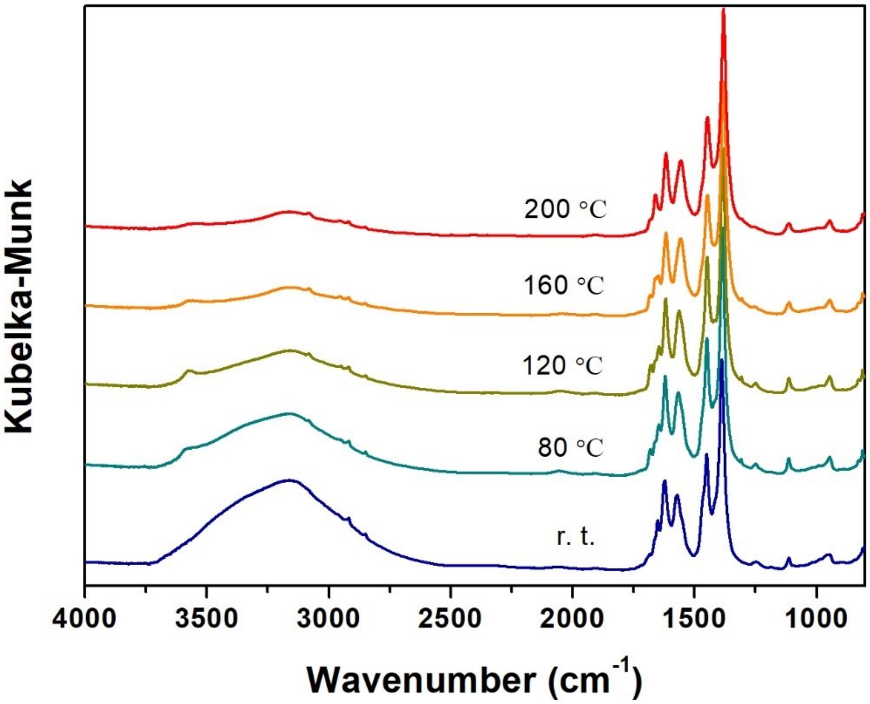

Figure S20. DRIFTS of **MOF-808-Br** under different temperatures in Ar atomosphere.

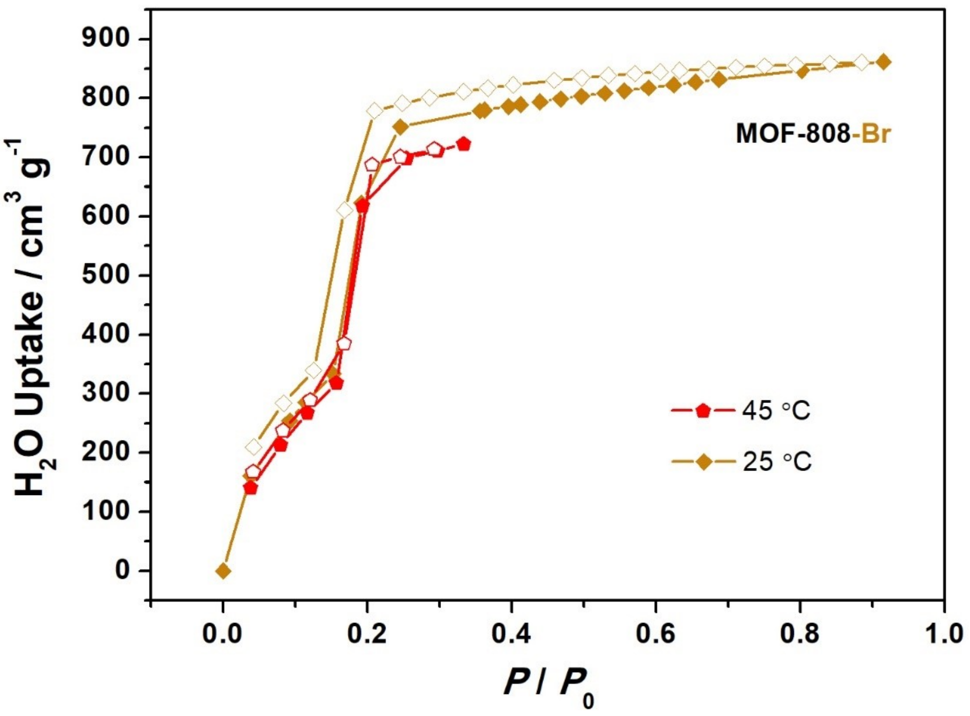

Figure S21. Water adsorption isotherms of **MOF-808-Br** at 25 °C and 45 °C.

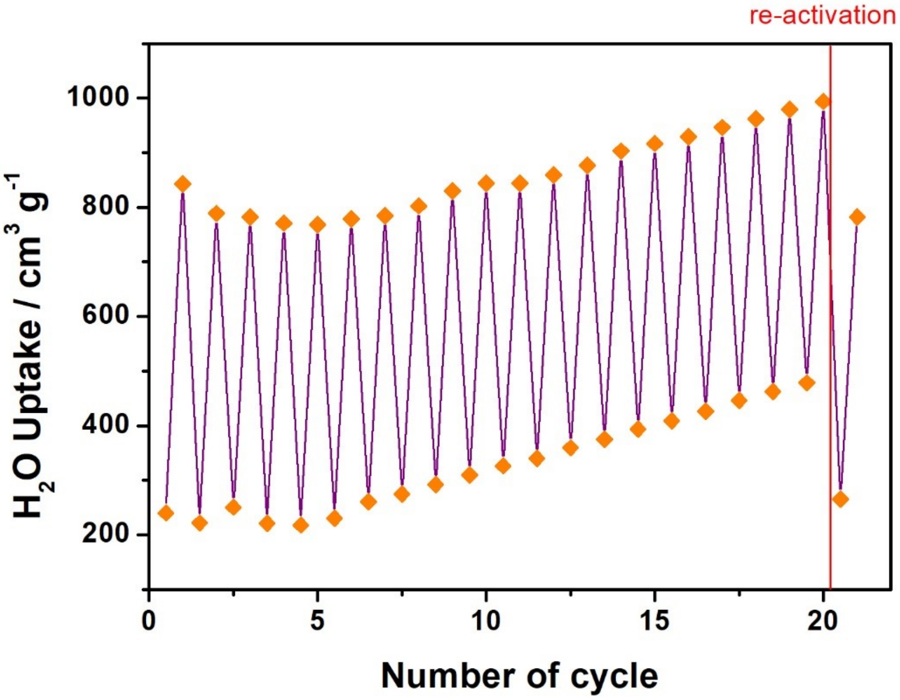

Figure S22. The two-points cycle stability test of **MOF-808-Br**; $P/P_0 = 0.1$ and 0.8, respectively. The 21st cycle was done after re-activation of the sample at 80 °C under dynamic vacuum for 12h.

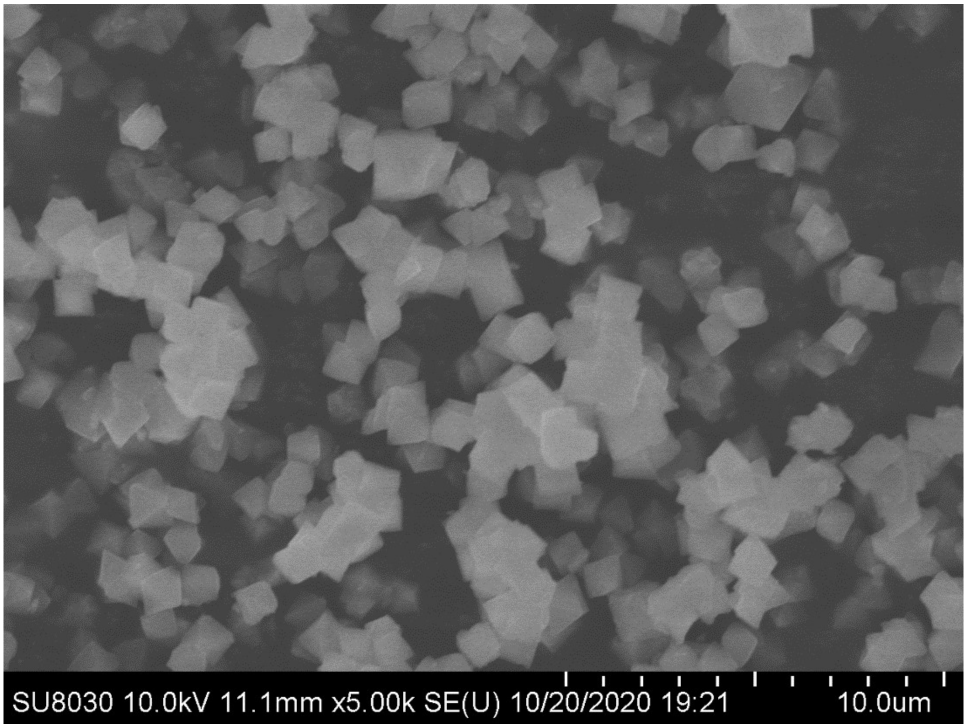

Figure S23. Scanning Electron Microscopy (SEM) image of **MOF-808-Br** after 20 cycles of water adsorption.

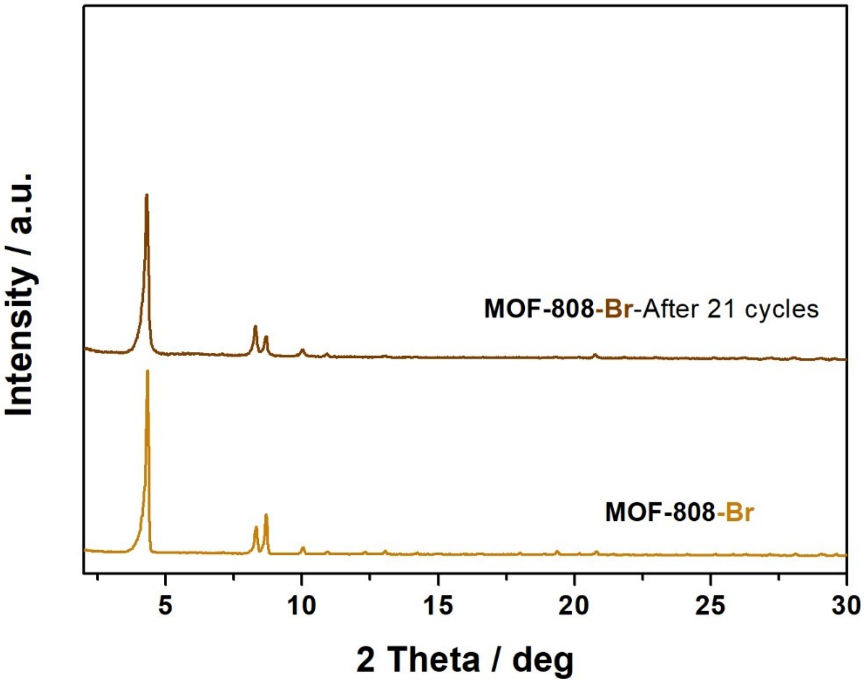

Figure S24. PXRD patterns of MOF-808-Br before water adsorption and after 21cycles of water adsortption.

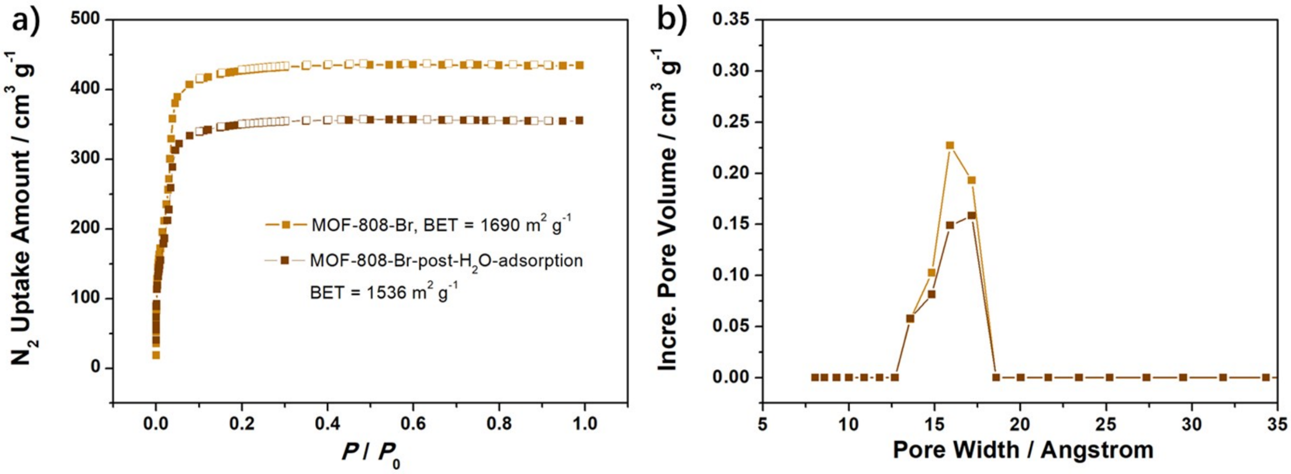

Figure S25. a) Nitrogen adsorption isotherms and b) Pore size distributions of **MOF-808-Br** and **MOF-808-Br** after 21 cycles of water adsorption.

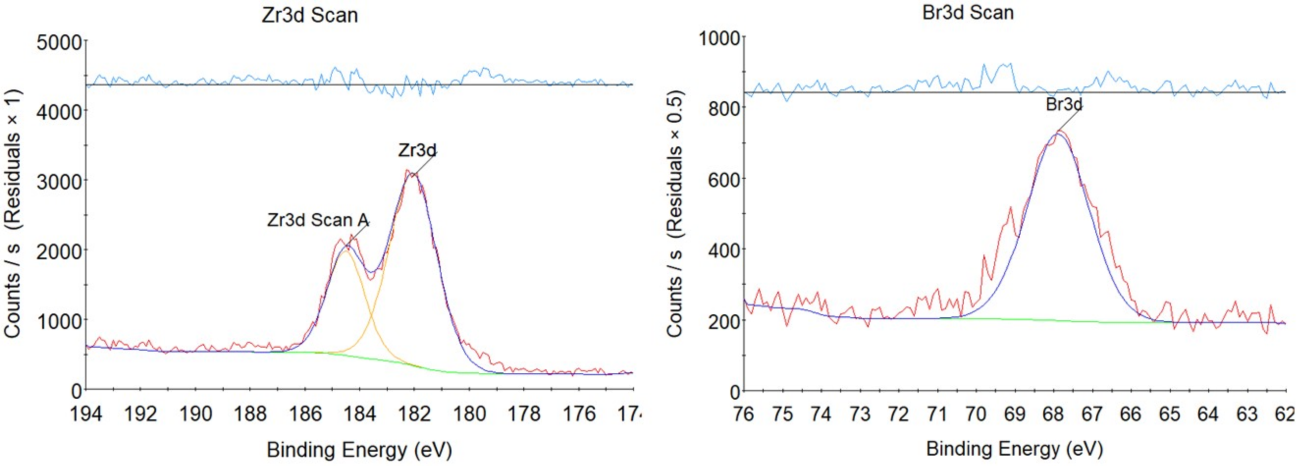

Figure S26. XPS of **MOF-808-Br**. The binding energy of Br is 67.9 eV.

5. MOF-808-I and its water adsorption

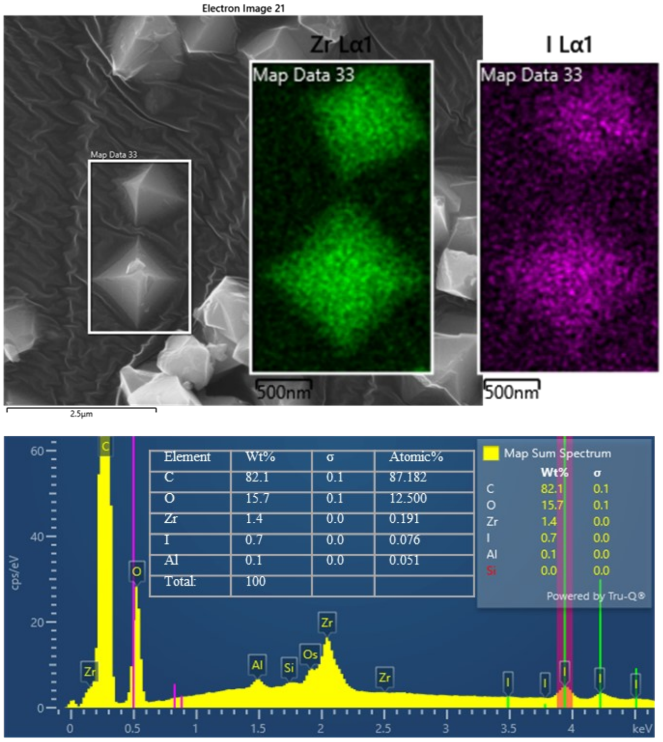

Element	Wt%	σ	Atomic%
C	82.1	0.1	87.182
O	15.7	0.1	12.500
Zr	1.4	0.0	0.191
I	0.7	0.0	0.076
Al	0.1	0.0	0.051
Total	100		

Map Sum Spectrum

	Wt%	σ
C	82.1	0.1
O	15.7	0.1
Zr	1.4	0.0
I	0.7	0.0
Al	0.1	0.0
Si	0.0	0.0

Powered by Tru-Q®

Figure S27. SEM-EDS mapping of **MOF-808-I** showing the evenly distribution of I.

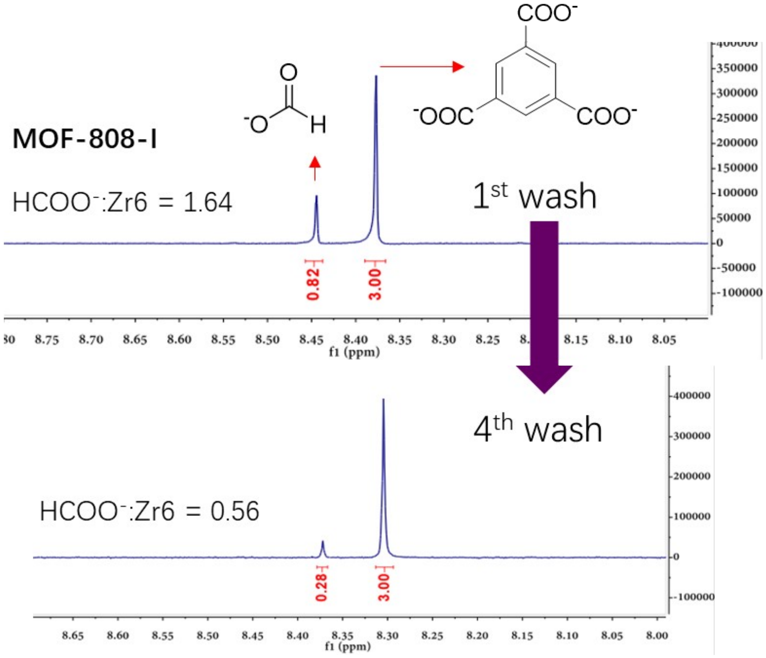

Figure S28. ^{1}H NMR spectrum of **MOF-808-I** digested in 0.1 M NaOD/D_2O and diluted in D_2O showing that even after repeating the HI washing for four times, there are still about 0.56 formate (at 8.37 ppm) left on each Zr_6 node.

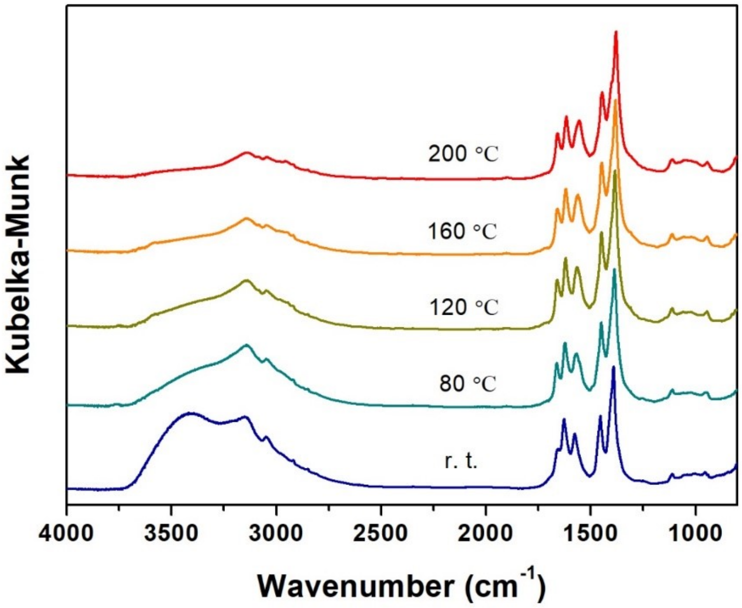

Figure S29. DRIFTS of **MOF-808-I** under different temperatures in Ar atomosphere.

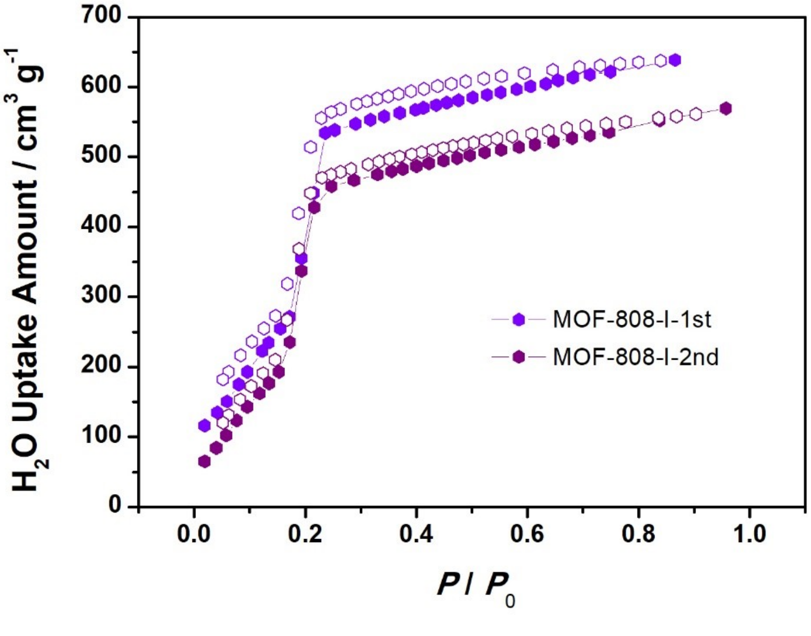

Figure S30. Water adsorption isotherms of **MOF-808-I** at 25 °C for two full cycles.

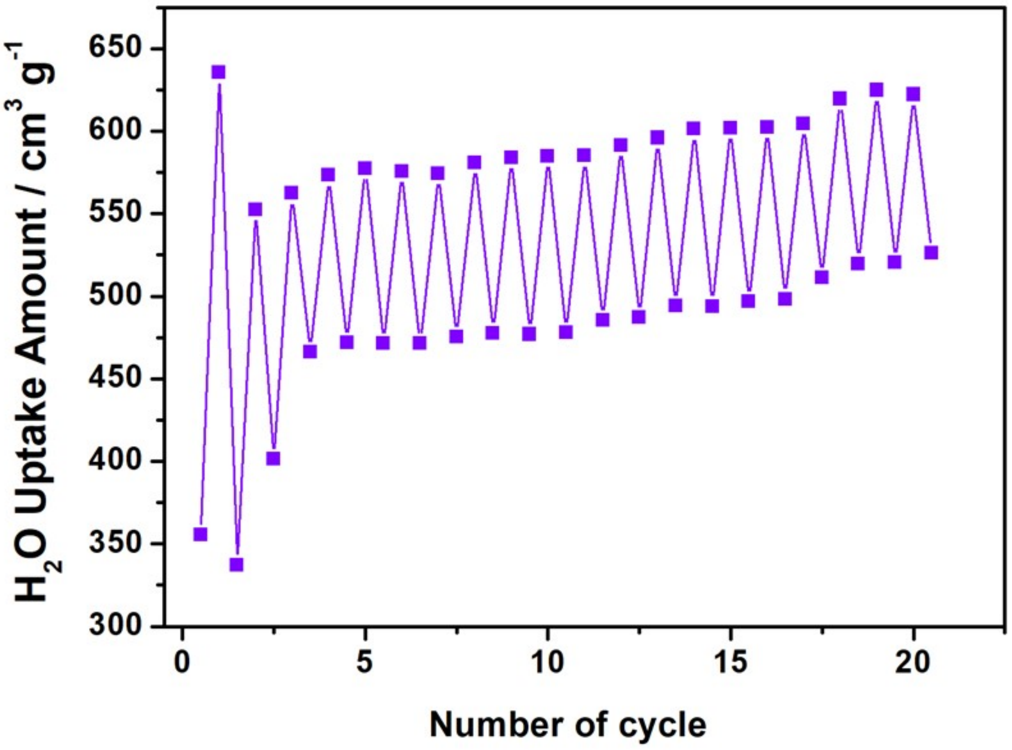

Figure S31. The two-points cycle stability test of **MOF-808-I**; P/P_0 = 0.2 and 0.9, respectively.

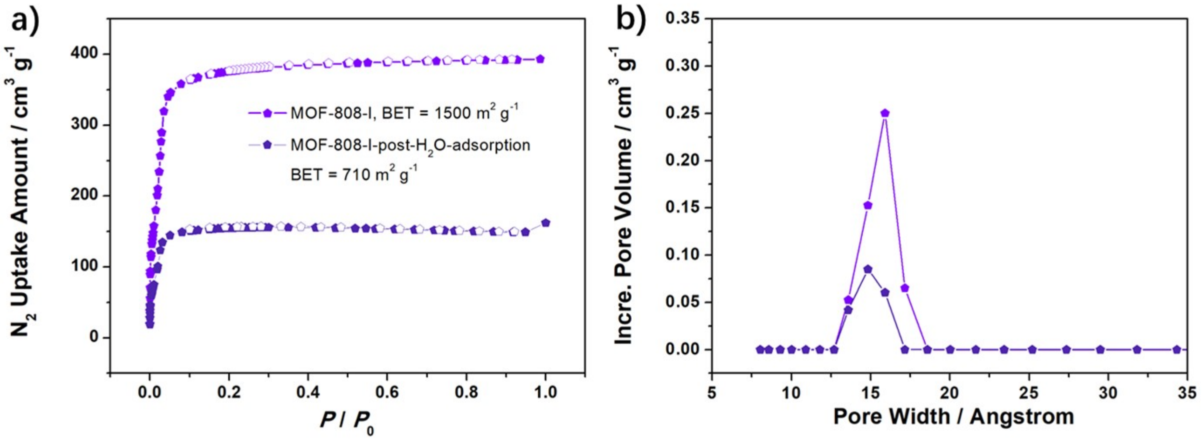

Figure S32. a) Nitrogen adsorption isotherms and b) Pore size distributions of **MOF-808-I** and **MOF-808-I** after 21 cycles of water adsorption.

6. MOF-808-Formate-free and its water adsorption

Preparation of MOF-808-Formate-free. 40 mg of MOF-808-Cl was solvent-exchanged with ethanol over the course of 12 h (4 × 10 mL) and kept in 10 mL ethanol. To the ethanol suspension of MOF-808-Cl, triethylamine (TEA, 11.2 μL, 0.08 mmol, about 3 equivalents to the Zr6 nodes of MOF-808) was added and kept for 18 h at room temperature. The material was then isolated by centrifugation and washed with ethanol, and the TEA wash was repeated. (For reasons that are unclear, a single wash with ~4 equivalents of TEA was less satisfactory.) The material was then isolated by centrifugation and washed five times with ethanol (~10 mL each). SEM-EDS (Scanning Electron Microscope-Energy Dispersive Spectroscopy) was used to monitor chlorine removal. If chlorine is not completely removed, additional washing with TEA wash can be done. Next, the sample was washed with acetone three times (~60 mL each; soaking ~1 h between washes) and soaked in acetone for an additional 16 h. Formate-free and Cl-free MOF-808 was collected by centrifugation, and then activated by supercritical CO_2 dryer to yield white powder.

Water adsorption of MOF-808-Formate-free. 30 mg of MOF-808-formate-free SCD-activated sample was transferred to adsorption sample tube in lab air, and thermal treated at 120 °C for 16 h under dynamic vacuum to remove coordinated aqua molecules before water adsorption. As shown in Figure S33, it turned out that MOF-808-Formate-free is not mechanically stable enough after the removal of coordinated water molecules, in comparison with MOF-808-Formate. Therefore, MOF-808-Formate-free shows a worse performance than MOF-808-Formate in the first cycle of water adsorption. Both of them end up with similar water uptakes in later cycles due to the collapse of frameworks.

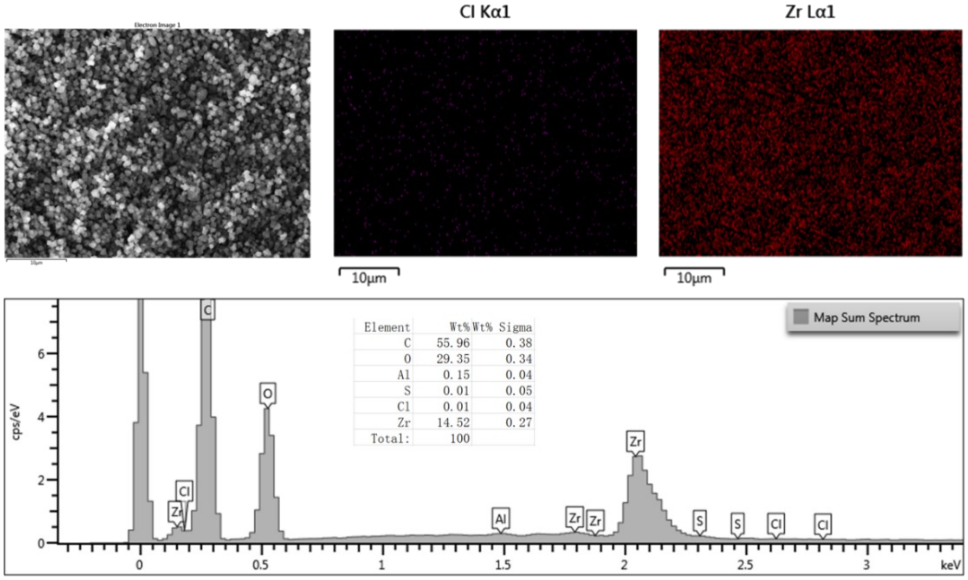

Element	Wt%	Wt% Sigma
C	55.96	0.38
O	29.35	0.34
Al	0.15	0.04
S	0.01	0.05
Cl	0.01	0.04
Zr	14.52	0.27
Total:	100	

Figure S33. SEM-EDS mapping of **MOF-808-formate-free** showing the completely removal of Cl.

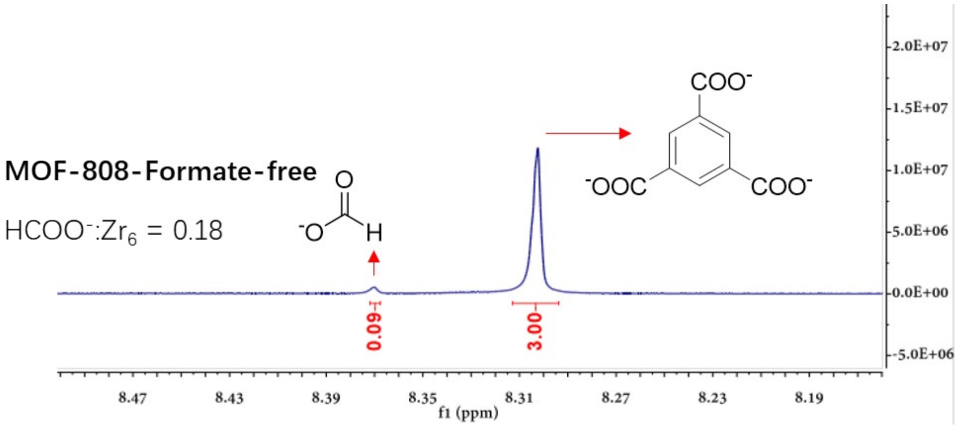

Figure S34. ^{1}H NMR spectrum of **MOF-808-Formate-free** digested in 0.1 M NaOD/D_2O and diluted in D_2O. There are about 0.18 formate (at 8.37 ppm) left on each Zr_6 node.

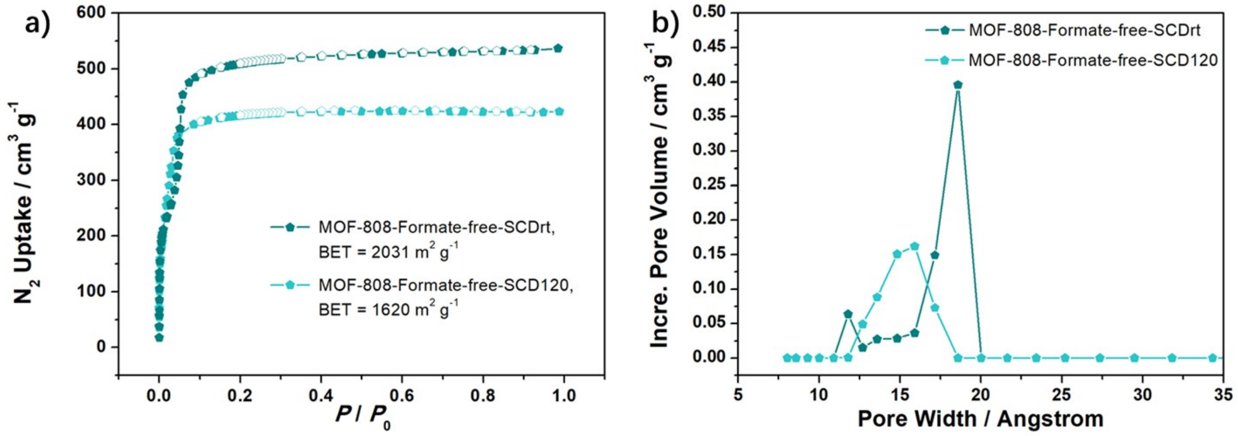

Figure S35. Nitrogen adsorption isotherms (a) and pore size distribution (b) of **MOF-808-Formate-free** activated by SCD and then evacuated at room temperature and 120 °C for 10 hours.

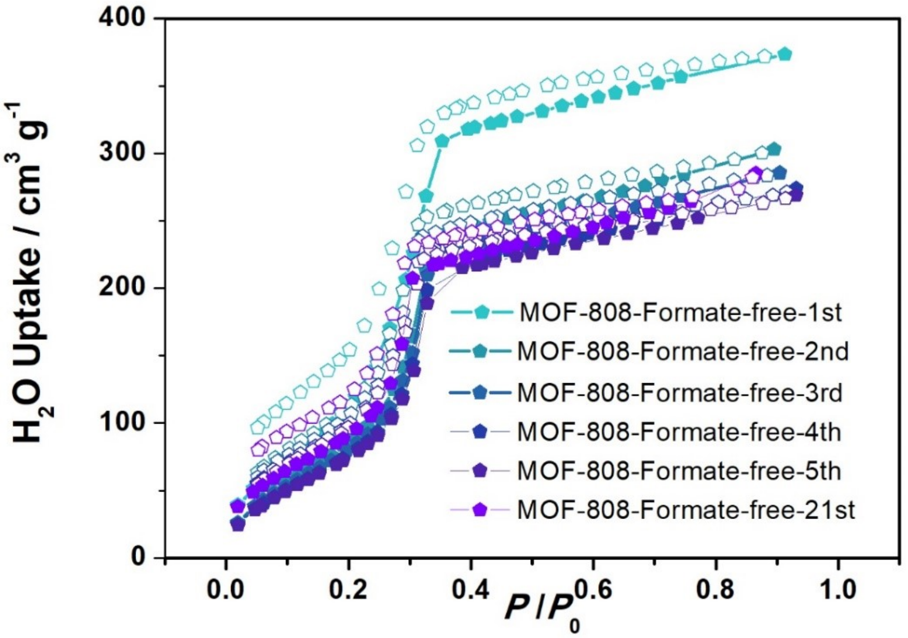

Figure S36. Water adsorption isotherms of **MOF-808-Formate-free** at 25 °C from the 1st cycle to the 21st cycle.

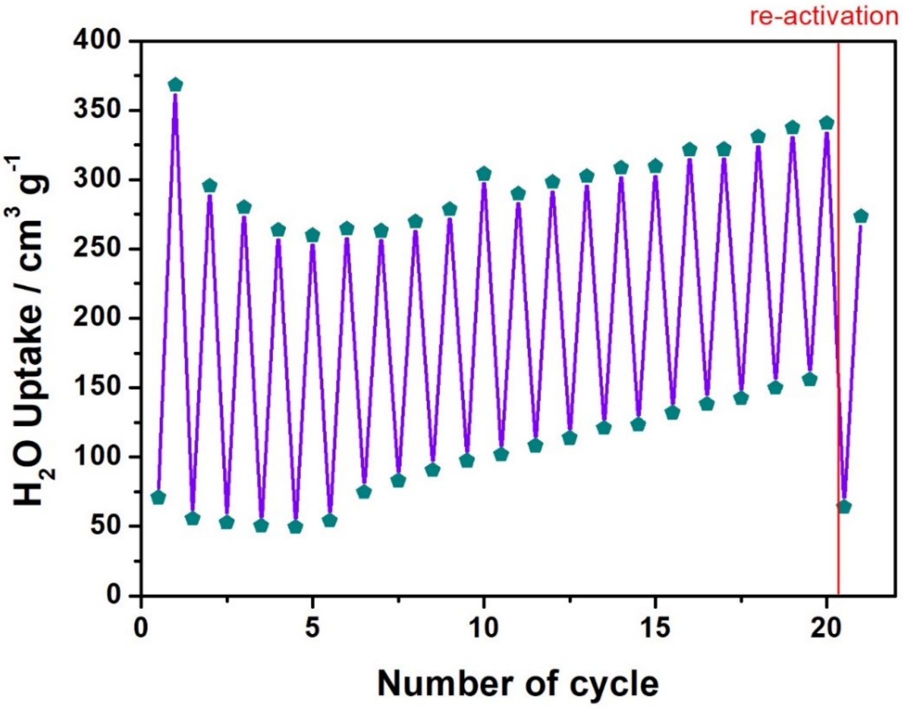

Figure S37. The two-points cycle stability test of **MOF-808-Formate-free**; P/P_0 = 0.1 and 0.8, respectively. The 21st cycle was done after re-activation of the sample at 80 °C under dynamic vacuum for 12h.

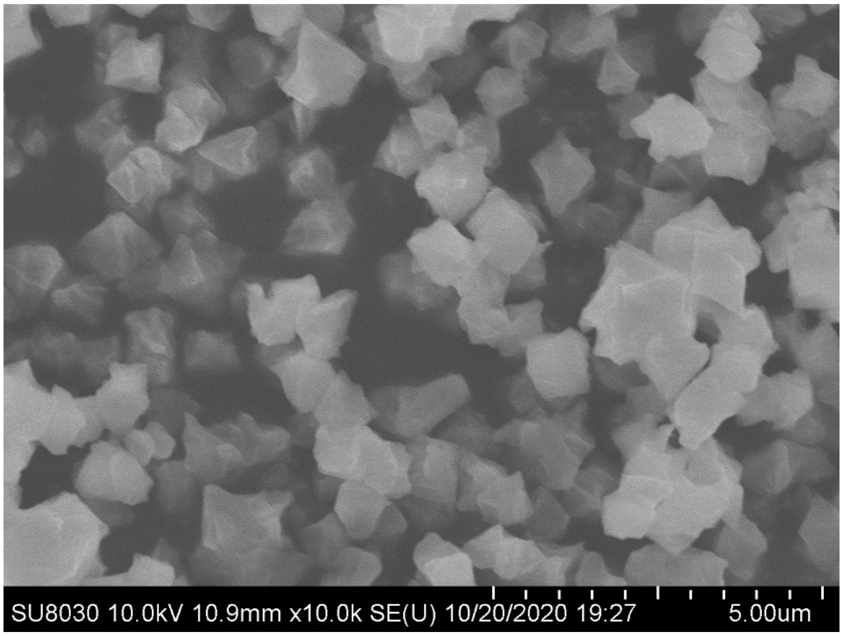

Figure S38. Scanning Electron Microscopy (SEM) image of **MOF-808-Formate-free** after 20 cycles of water adsorption.

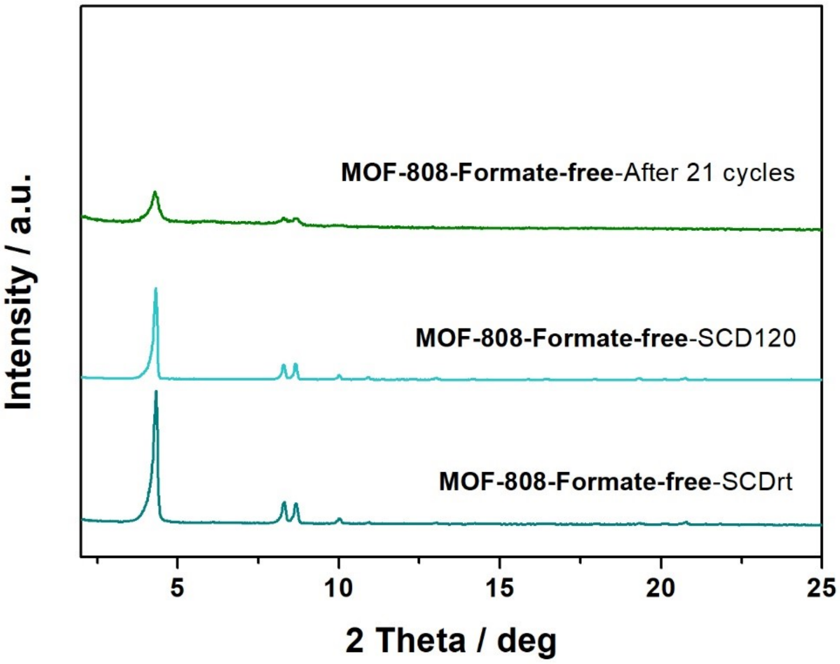

Figure S39. PXRD patterns of MOF-808-Formate-free before water adsorption and after 21 cycles of water adsorption.

7. Comparison

Table S1 Saturated Water Capacities for Selected MOFs

MOFs	**α**[a] **(% RH)**	q_{max} **(g g**$^{-1}$**)**	q_{max} **(cm**^{3} **g**$^{-1}$**)**	**Crystal ρ (g cm**$^{-3}$**)**	q_{vmax} **(cm**^{3} **cm**$^{-3}$**)**	**Reference**
MOF-808-Br	16	0.693	862	1.200	1033	This work
MIL-101(Cr)	40	1.73	2153	0.451	971	[2]
Cr-soc-MOF-1	69	1.95	2427	0.381	924	[3]
$Ni_8(L5)_6$	70	1.12	1394	0.64	892	[4]
Co_2Cl_2(BTDD)	29	0.97	1207	0.706	852	[5]
$Ni_8(L3)_6$	40	0.99	1232	0.69	850	[4]
MOF-808-I	18	0.517	643	1.286	827	This work
MOF-808-Cl	16	0.746	928	0.886	823	This work
MOF-74(Ni)-BPP	23	0.81	1008	0.808	814	[6]
MOF-74(Ni)-TPP	50	0.9	1120	0.664	744	[6]
NU-1500-Cr	48	1.09	1360	0.533	725	[7]
Zn_2Co_3(MFU-4l)	40	1.11	1381	0.519	717	[8]
MIL-101(Cr)-SO_3H	28	0.95	1182	0.605	715	[9]
$Ni_8(L5\text{-}CF_3)_6$	85	0.86	1070	0.65	696	[4]
NU-1000	75	1.14	1419	0.490	695	[10]
Zn_5(MFU-4l)	65	1.04	1294	0.527	682	[8]
UiO-66	36	0.44	547	1.23	673	[1]
MOF-841	26	0.51	635	1.05	666	[1]
DUT-67	37	0.5	622	1.06	660	[1]
MIL-101(Cr)-	42	1.05	1307	0.480	627	[11]

NH_2						
Zn_3Co_2(MFU-4l)	44	0.95	1182	0.522	617	8
(Mg)MOF-74	5	0.54	672	0.91	612	12
Y-shp-MOF-5	64	0.5	622	0.97	604	13
MIL-101(Cr)-$p$$NH_2$	41	1 (293K)	1244	0.474	590	14
NU-1003	77	1.5	1867	0.306	571	15

[a] α is the % RH at which half of the total uptake at 90~95% RH is reached

Table S2 Water Capacities for Selected Porous Materials with α at or below 30% RH

MOFs	**α[a] (% RH)**	**Uptake (cm^3 g^{-1})**	**Crystal ρ (g cm^{-3})**	**Uptake (cm^3 cm^{-3})**	**Reference**
MOF-808-Br	30	770	1.199	923	This work
Ni_2Br_2BTDD	24	946	0.764	723	16
MOF-808-Cl	30	802	0.893	716	This work
MOF-808-I	30	552	1.280	707	This work
MOF-303	15	597	1.159	692	17
ALPO-78	18	398	1.7	677	18
MOF-841	22	635	1.05	666	1
MIP-200	18	560	1.16	650	19
Ti-MIL-125-NH_2	23	846	0.757	641	20
MOF-801	9	348	1.59	554	1
Ni_2Cl_2BBTA	3	498	1.1	548	16
CAU-10	18	473	1.15	544	21
AQSOA Z02	8	373	1.43	534	22

MIL-160	8	460	1.15	530	[23]
AQSOA Z05	25	224	1.75	392	[22]
AQSOA Z01	17	224	1.75	392	[22]

[a] α is the % RH at which half of the total uptake at 90~95% RH is reached

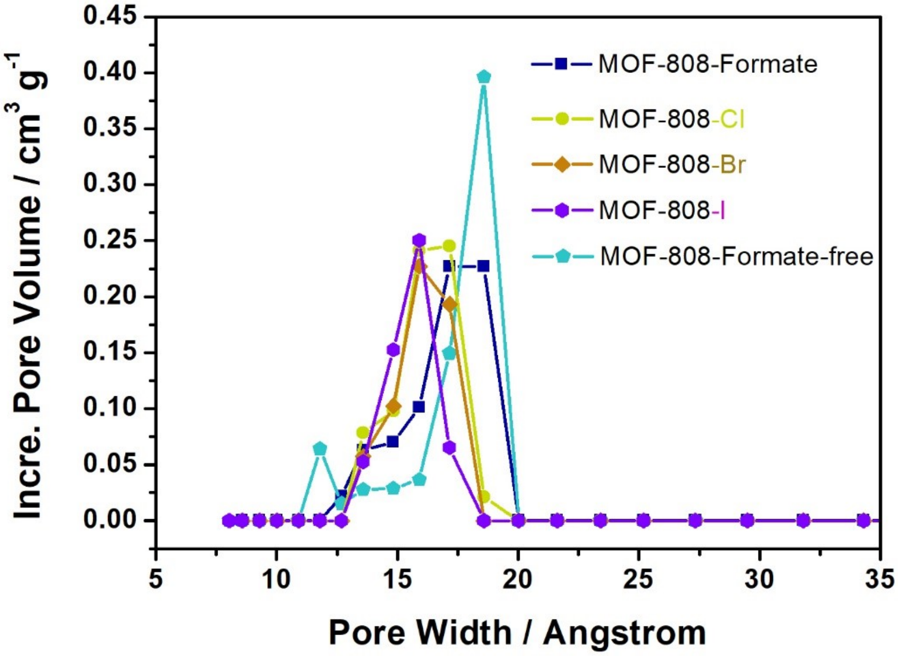

Figure S40. Pore size distribution of **MOF-808** series.

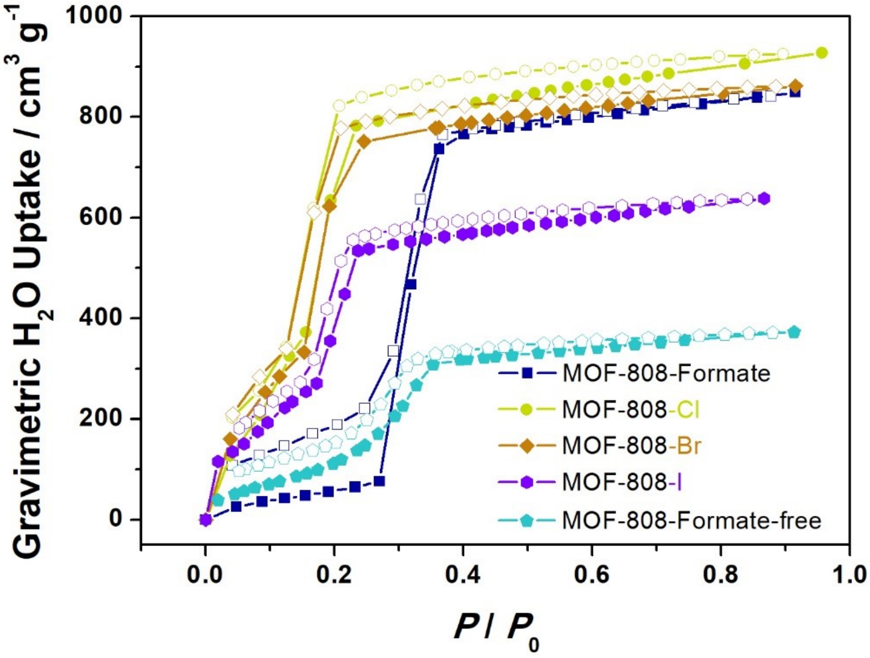

Figure S41. Gravimetric water adsorption isotherms of **MOF-808** series at 25 °C.

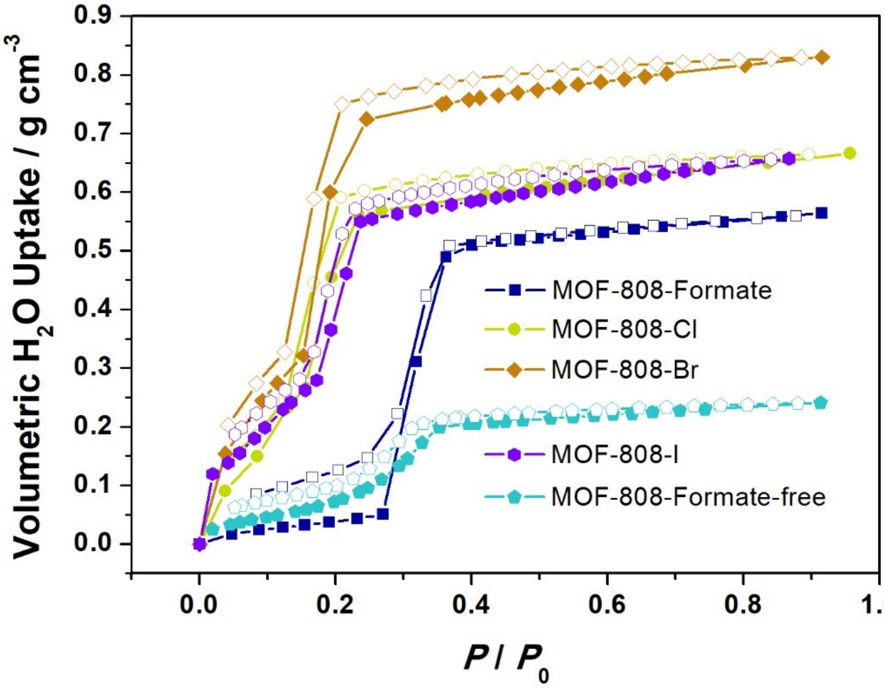

Figure S42. Volumetric water adsorption isotherms of **MOF-808** series at 25 °C.

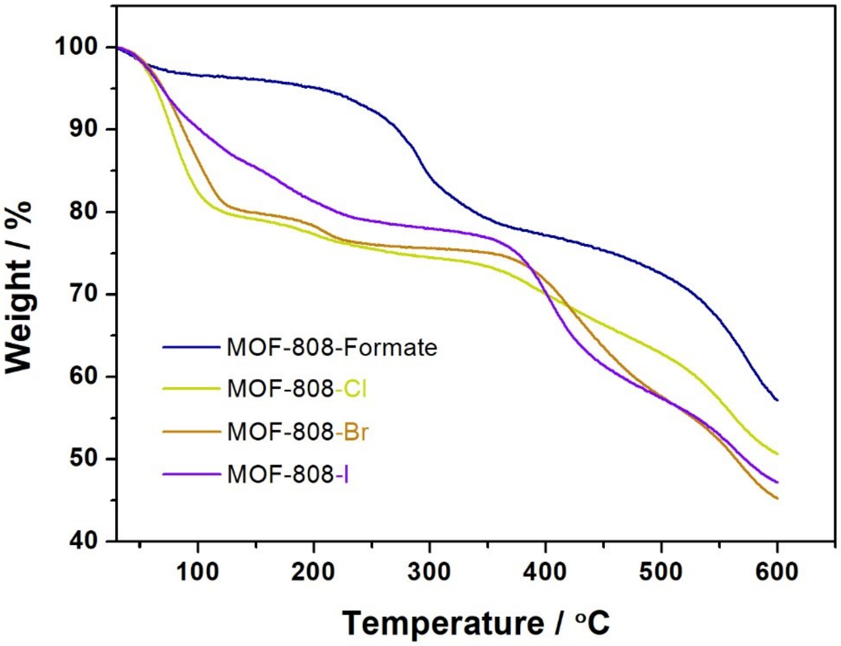

Figure S43. TG curves of **MOF-808** series.

8. References

(1) Furukawa, H.; Gandara, F.; Zhang, Y. B.; Jiang, J.; Queen, W. L.; Hudson, M. R.; Yaghi, O. M. Water adsorption in porous metal-organic frameworks and related materials. *J Am Chem Soc* **2014,** *136* (11), 4369.
(2) De Lange, M. F.; Gutierrez-Sevillano, J.-J.; Hamad, S.; Vlugt, T. J. H.; Calero, S.; Gascon, J.; Kapteijn, F. Understanding Adsorption of Highly Polar Vapors on Mesoporous MIL-100(Cr) and MIL-101(Cr): Experiments and Molecular Simulations. *J Phys Chem C* **2013,** *117* (15), 7613.
(3) Towsif Abtab, S. M.; Alezi, D.; Bhatt, P. M.; Shkurenko, A.; Belmabkhout, Y.; Aggarwal, H.; Weseliński, Ł. J.; Alsadun, N.; Samin, U.; Hedhili, M. N.et al. Reticular Chemistry in Action: A Hydrolytically Stable MOF Capturing Twice Its Weight in Adsorbed Water. *Chem* **2018,** *4* (1), 94.
(4) Padial, N. M.; Quartapelle Procopio, E.; Montoro, C.; Lopez, E.; Oltra, J. E.; Colombo, V.; Maspero, A.; Masciocchi, N.; Galli, S.; Senkovska, I.et al. Highly hydrophobic isoreticular porous metal-organic frameworks for the capture of harmful volatile organic compounds. *Angew Chem Int Ed Engl* **2013,** *52* (32), 8290.
(5) Rieth, A. J.; Yang, S.; Wang, E. N.; Dinca, M. Record Atmospheric Fresh Water Capture and Heat Transfer with a Material Operating at the Water Uptake Reversibility Limit. *ACS Cent Sci* **2017,** *3* (6), 668.
(6) Zheng, J.; Vemuri, R. S.; Estevez, L.; Koech, P. K.; Varga, T.; Camaioni, D. M.; Blake, T. A.; McGrail, B. P.; Motkuri, R. K. Pore-Engineered Metal-Organic Frameworks with Excellent Adsorption of Water and Fluorocarbon Refrigerant for Cooling Applications. *J Am Chem Soc* **2017,** *139* (31), 10601.
(7) Chen, Z.; Li, P.; Zhang, X.; Li, P.; Wasson, M. C.; Islamoglu, T.; Stoddart, J. F.; Farha, O. K. Reticular Access to Highly Porous acs-MOFs with Rigid Trigonal Prismatic Linkers for Water Sorption. *J Am Chem Soc* **2019,** *141* (7), 2900.

(8) Wright, A. M.; Rieth, A. J.; Yang, S.; Wang, E. N.; Dinca, M. Precise control of pore hydrophilicity enabled by post-synthetic cation exchange in metal-organic frameworks. *Chem Sci* **2018,** *9* (15), 3856.
(9) Akiyama, G.; Matsuda, R.; Sato, H.; Hori, A.; Takata, M.; Kitagawa, S. Effect of functional groups in MIL-101 on water sorption behavior. *Micropor Mesopor Mat* **2012,** *157*, 89.
(10) Deria, P.; Chung, Y. G.; Snurr, R. Q.; Hupp, J. T.; Farha, O. K. Water stabilization of Zr6-based metal-organic frameworks via solvent-assisted ligand incorporation. *Chem Sci* **2015,** *6* (9), 5172.
(11) Khutia, A.; Rammelberg, H. U.; Schmidt, T.; Henninger, S.; Janiak, C. Water Sorption Cycle Measurements on Functionalized MIL-101Cr for Heat Transformation Application. *Chem Mater* **2013,** *25* (5), 790.
(12) Schoenecker, P. M.; Carson, C. G.; Jasuja, H.; Flemming, C. J. J.; Walton, K. S. Effect of Water Adsorption on Retention of Structure and Surface Area of Metal–Organic Frameworks. *Ind Eng Chem Res* **2012,** *51* (18), 6513.
(13) AbdulHalim, R. G.; Bhatt, P. M.; Belmabkhout, Y.; Shkurenko, A.; Adil, K.; Barbour, L. J.; Eddaoudi, M. A Fine-Tuned Metal-Organic Framework for Autonomous Indoor Moisture Control. *J Am Chem Soc* **2017,** *139* (31), 10715.
(14) Ko, N.; Choi, P. G.; Hong, J.; Yeo, M.; Sung, S.; Cordova, K. E.; Park, H. J.; Yang, J. K.; Kim, J. Tailoring the water adsorption properties of MIL-101 metal–organic frameworks by partial functionalization. *J Mater Chem A* **2015,** *3* (5), 2057.
(15) Lv, X. L.; Yuan, S.; Xie, L. H.; Darke, H. F.; Chen, Y.; He, T.; Dong, C.; Wang, B.; Zhang, Y. Z.; Li, J. R.et al. Ligand Rigidification for Enhancing the Stability of Metal-Organic Frameworks. *J Am Chem Soc* **2019,** *141* (26), 10283.
(16) Rieth, A. J.; Wright, A. M.; Skorupskii, G.; Mancuso, J. L.; Hendon, C. H.; Dinca, M. Record-Setting Sorbents for Reversible Water Uptake by Systematic Anion Exchanges in Metal-Organic Frameworks. *J Am Chem Soc* **2019,** *141* (35), 13858.
(17) Fathieh, F.; Kalmutzki, M. J.; Kapustin, E. A.; Waller, P. J.; Yang, J.; Yaghi, O. M. Practical water production from desert air. *Sci Adv* **2018,** *4* (6), eaat3198.
(18) Yuhas, B. D.; Mowat, J. P. S.; Miller, M. A.; Sinkler, W. AlPO-78: A 24-Layer ABC-6 Aluminophosphate Synthesized Using a Simple Structure-Directing Agent. *Chem Mater* **2018,** *30* (3), 582.
(19) Wang, S.; Lee, J. S.; Wahiduzzaman, M.; Park, J.; Muschi, M.; Martineau-Corcos, C.; Tissot, A.; Cho, K. H.; Marrot, J.; Shepard, W.et al. A robust large-pore zirconium carboxylate metal–organic framework for energy-efficient water-sorption-driven refrigeration. *Nat Energy* **2018,** *3* (11), 985.
(20) Sohail, M.; Yun, Y.-N.; Lee, E.; Kim, S. K.; Cho, K.; Kim, J.-N.; Kim, T. W.; Moon, J.-H.; Kim, H. Synthesis of Highly Crystalline NH2-MIL-125 (Ti) with S-Shaped Water Isotherms for Adsorption Heat Transformation. *Cryst Growth Des* **2017,** *17* (3), 1208.
(21) Fröhlich, D.; Pantatosaki, E.; Kolokathis, P. D.; Markey, K.; Reinsch, H.; Baumgartner, M.; van der Veen, M. A.; De Vos, D. E.; Stock, N.; Papadopoulos, G. K.et al. Water adsorption behaviour of CAU-10-H: a thorough investigation of its structure–property relationships. *Journal of Materials Chemistry A* **2016,** *4* (30), 11859.
(22) de Lange, M. F.; Verouden, K. J.; Vlugt, T. J.; Gascon, J.; Kapteijn, F. Adsorption-Driven Heat Pumps: The Potential of Metal-Organic Frameworks. *Chem Rev* **2015,** *115* (22), 12205.
(23) Cadiau, A.; Lee, J. S.; Damasceno Borges, D.; Fabry, P.; Devic, T.; Wharmby, M. T.; Martineau, C.; Foucher, D.; Taulelle, F.; Jun, C. H.et al. Design of hydrophilic metal organic framework water adsorbents for heat reallocation. *Adv Mater* **2015,** *27* (32), 4775.